Stabilising and destabilising effects of polarisation dynamics in class C lasers with optical external injection or time-delayed feedback.

Sebastian Wieczorek[1] and Weng W. Chow[2,3],
[1] *Mathematics Research Institute, CEMPS, University of Exeter, EX4 4QF, UK,*
[2] *Sandia National Laboratories, Albuquerque, New Mexico 87185-1086, USA,*
[3] *Physics Dept. and Institute of Quantum Studies, Texas A&M University, College Station, Texas 77843, USA.*
(July 8, 2013)

ABSTRACT

This paper examines laser stability during transition between class B and class C conditions, when polarisation dynamics changes to evolving on a similar timescale as the population inversion and laser intensity. Numerical and analytical studies, based on the Maxwell-Bloch equations, indicate that class C conditions can stabilise or destabilise a laser. The former effect is counter-intuitive and is demonstrated using examples of optical injection and time-delayed feedback, where externally induced instabilities and chaos found for class B conditions disappear for class C conditions. A systematic parametric study identifies combinations of laser parameters, i.e. the excitation rate, cavity detuning and ratio of laser-field to population-inversion decay rates, giving rise to the two opposite results of transitioning from class B to class C operation.

I. INTRODUCTION

Studies of nonlinear laser dynamics date back to 1970's. Since then, there has been an impressive growth in activities for two reasons. One reason is that lasers provide an excellent experimental platform for exploring new and exciting nonlinear dynamics. Strong optical nonlinearities combine with weak dissipation to make lasers very susceptible to external disturbances. For example, laser operation may destabilise with optical feedback, resulting in rich displays of regular or erratic (e.g. chaotic) intensity oscillations. Similar destabilisation also occurs with external optical injection [1,2], optoelectronic feedback [3] and coupling to another laser [4–7]. The second reason is that nonlinear dynamics has been very successful in improving our knowledge of laser dynamical behaviour [8–15] and stimulating novel applications [16,21–23]. Practically every laser application is impacted by dynamical performance. For example, high-speed response is important for optical communication [17,18], while dynamical stability is essential for spectroscopy.

The evolution of the study of laser dynamics into a major discipline owes much to the fact that important laser nonlinearities can be captured accurately and concisely with the Maxwell-Bloch equations [19,20]. These differential equations describe the time evolutions of the complex-valued intracavity electric field, complex-valued active-medium polarisation and real-valued active-medium population inversion [8,10]. The advantages are maintained even when the equations become non autonomous and involve time-delayed influences in the presence of external disturbances. To date, the Maxwell-Bloch equations continue to allow in-depth stability analysis, using modern numerical and theoretical concepts from dynamical systems and bifurcation theory [13,14,24,25].

Depending on the active medium and optical cavity, the three laser variables (laser electric field, active medium polarisation and population inversion) evolve with separate timescales, subjected to one constraint — population dynamics cannot be faster than polarisation dynamics

owing to the influence of dephasing on the latter [8, Ch.7]. Based on the relationships among these timescales, a laser can be categorised into three classes: *class A, class B and class C* [26]. Initial theoretical studies of laser instabilities [8,11] were focused on class C laser models, where the full set of Maxwell-Bloch equations were used. With the arrival of semiconductor lasers in the 1980's, the focus shifted to class B laser models, which involved only the differential equations for electric field and population inversion [27, Ch.3] This simplification is possible because fast dephasing allowed adiabatic elimination of the polarisation differential equation. Majority of results on laser instabilities and chaos in response to optical injection or feedback are obtained using class B laser models.

Recent technological advances, such as those leading to quantum-dot (QD) lasers [28] and quantum-cascade lasers (QCLs) [29], give reason for revisiting class C laser models. The reason is that fundamental changes in the active medium or laser transition make elimination of the polarisation equation no longer always possible. In QD lasers, reduced scattering under conditions such as low temperature, may decrease dephasing rates so that polarisation dynamics is slowed to being comparable with population dynamics. In a QCL, laser action and thus population dynamics involve intersubband transitions. A consequence is that population inversion can change at the ultra fast rate of intraband collisions, which also govern polarisation dynamics. These can lead to polarisation, population and radiation field amplitude all changing on comparable time scales. In both cases (whether it is polarisation dynamics slowing down or population dynamics speeding up), the question of externally-induced instabilities or bifurcations has not been fully addressed.

This paper is motivated by the general need to better understand effects of class C conditions on laser stability. The case of a single-mode laser is used to demonstrate possible effects of approaching class C conditions from class B ones. Of interest are changes in the number and type of lasing solutions and the stability of these solutions. Moreover, whether the solutions describe stabilisation or destabilisation of laser operation have practical relevance. To quantify the difference, we introduce and explain the concept of relative stability difference and illustrate its use in a systematic parametric study for identifying combinations of laser parameters (laser-field and population decay rates, excitation rate and detuning) leading to either stabilisation or destabilisation.

We present counter-intuitive results showing suppression of laser instabilities as the ratio of polarisation and laser-field decay rates decreases towards class C conditions in two laser configurations. For a laser subject to optical injection, we show that regions of bistability shrink noticeably and some bifurcations leading to stable field-amplitude oscillations disappear from the stability diagram. For a laser subject to time-delayed optical feedback, we show an even stronger effect where all type (periodic and chaotic) field-amplitude oscillations are suppressed. The end result is a stability diagram that is highly multistable but devoid of any amplitude instabilities.

Section II describes the class C laser model. Section III identifies parameter regimes where stability of a solitary laser either decreases or increases when transitioning from class B to class C conditions. A systematic parametric study is used to identify different possible scenarios with dependencies on the ratio of field and population decay rates, excitation rate and detuning between cavity and transition frequencies. Guided by the solitary laser results, Sections IV and V explore the less intuitive stabilising effects of class C conditions on two canonical laser configurations in nonlinear dynamics: laser with external optical injection and laser with time-delayed optical feedback. Generalisations are made to the class B formulae for phase-locked or rotating-wave solutions of the two configurations [32,25] by including terms arising from polarisation dynamics. In these studies, we first obtain analytical formulae for steady-state lasing solutions, identify the new terms arising from polarisation dynamics and compute the

bifurcations leading to field-amplitude oscillations. Then, we analyse changes to externally-induced multistability and instabilities when approaching class C conditions.

II. CLASS C LASER MODEL

We consider a laser with a homogeneously broadened two-level active medium inside a Fabry-Perot cavity. Assuming that only one cavity mode lies within the gain bandwidth, we write for the laser electric field $E(z,t)$ and active-medium polarisation $P(z,t)$, [8]

$$E(z,t) = \frac{1}{2}u(z)\left[\mathcal{E}(t)e^{-i\nu t} + \mathcal{E}^*(t)e^{i\nu t}\right], \tag{1}$$

$$P(z,t) = \frac{1}{2}u(z)\left[\mathcal{P}(t)e^{-i\nu t} + \mathcal{P}^*(t)e^{i\nu t}\right], \tag{2}$$

where $u(z)$ is the passive-cavity mode, z is position along the optical cavity axis and ν is an optical frequency chosen to facilitate the calculations, as explained in Sections III–V. The complex slowly-varying amplitudes for the electric field and polarisation are $\mathcal{E}(t) = |\mathcal{E}(t)|\exp(i\varphi(t))$ and $\mathcal{P}(t)$, respectively, and the lasing frequency is $\nu + d\varphi/dt$.

With the above expressions for laser field and active-medium polarisation, dynamics of a class C laser is governed by the Maxwell-Bloch equations [8,30]:

$$\frac{d\mathcal{E}}{dt} = -\gamma_c\mathcal{E} - i(\Omega-\nu)\mathcal{E} + \frac{i\nu}{2\epsilon}\mathcal{P} + f(t), \tag{3}$$

$$\frac{d\mathcal{P}}{dt} = -\gamma_p\mathcal{P} + i(\omega-\nu)\mathcal{P} - \frac{i\wp^2}{\hbar}\Gamma\bar{N}\mathcal{E}, \tag{4}$$

$$\frac{d\bar{N}}{dt} = \lambda - \gamma_n\bar{N} - \frac{i}{2\hbar\Gamma}(\mathcal{E}^*\mathcal{P} - \mathcal{E}\mathcal{P}^*), \tag{5}$$

where $\bar{N}$ is the spatially-averaged population inversion density, Γ is the mode confinement factor, $\wp$ is the electric-dipole matrix element, and ϵ is the background permittivity. Also in the above equations are loss contributions containing laser-field decay rate γ_c (we often refer to the cavity or intensity decay rate $2\gamma_c$), dephasing rate γ_p and population decay rate γ_n. The pump rate is λ, passive-cavity mode frequency is Ω and active-medium transition frequency is ω. To include the possibility of optical injection or feedback, we added a forcing term $f(t)$ in (3). Equations (3)–(5) are invariant under rotation

$$(\mathcal{E},\mathcal{P},\bar{N},f) \to (\mathcal{E}e^{i\xi},\mathcal{P}e^{i\xi},\bar{N},fe^{i\xi}), \tag{6}$$

where $\xi \in (0,2\pi]$.

From among the many laser parameters, only a few are relevant to laser stability and nonlinear dynamics. To identify the relevant parameter combinations and to facilitate calculations, we rewrite class C laser model (3)–(5) in a dimensionless form

$$\dot{E} = -(1+i\Delta_c)E + iP + F(\tau), \tag{7}$$

$$\frac{1}{\gamma_{pc}}\dot{P} = -(1+i\Delta_p)P - iEN, \tag{8}$$

$$\frac{1}{\gamma_{nc}}\dot{N} = \Lambda - N - \frac{i}{2}(E^*P - EP^*), \tag{9}$$

where the dot indicates the first derivative with respect to normalised time $\tau = \gamma_c t$. The normalised quantities are $E = \mathcal{E}/\mathcal{E}_0$, $P = \mathcal{P}/\mathcal{P}_0$, $N = \bar{N}/N_0$ and $F(\tau) = f(\tau)\left(\mathcal{E}_0\gamma_c\right)^{-1}$, where

$$\mathcal{E}_0 = \frac{\hbar\sqrt{\gamma_n\gamma_p}}{\wp}, \tag{10}$$

$$\mathcal{P}_0 = \frac{2\hbar\epsilon\gamma_c\sqrt{\gamma_n\gamma_p}}{\wp\nu}, \tag{11}$$

$$N_0 = \frac{\mathcal{E}_0\mathcal{P}_0}{\hbar\Gamma\gamma_n}. \tag{12}$$

The rescaled detunings, decay rates and pump rate are

$$\Delta_c := \Delta_c(\nu) = \frac{\Omega-\nu}{\gamma_c}, \tag{13}$$

$$\Delta_p := \Delta_p(\nu) = \frac{\omega-\nu}{\gamma_p}, \tag{14}$$

$$\gamma_{pc} = \frac{\gamma_p}{\gamma_c}, \gamma_{nc} = \frac{\gamma_n}{\gamma_c} \text{ and } \Lambda = \frac{\lambda}{\gamma_n N_0}, \tag{15}$$

of which Δ_c and Δ_p depend on the choice of ν in (1) and (2).

To make connection to the class B limit, we formally integrate (8) to obtain

$$P(\tau) = e^{-\gamma_{pc}(1+i\Delta_p)\tau}\left[P(0) - i\gamma_{pc}\int_0^\tau ds\, E(s)\, N(s)\, e^{\gamma_{pc}(1+i\Delta_p)s}\right]. \tag{16}$$

In the limit that the elctric field amplitude and population inversion vary negligibly during the decay of the exponential containing γ_{pc}, and that $e^{-\gamma_{pc}\tau} \ll 1$, the integration may be performed by assuming

$$\begin{aligned} P(\tau) &\simeq e^{-\gamma_{pc}(1+i\Delta_p)\tau}\left[P(0) - i\gamma_{pc}E(\tau)\, N(\tau)\int_0^\tau ds\, e^{\gamma_{pc}(1+i\Delta_p)s}\right] \\ &\simeq -iE(\tau)\, N(\tau)\,(1-i\Delta_p)\mathcal{L}(\Delta_p), \end{aligned} \tag{17}$$

where we defined a dimensionless Lorentzian function,

$$\mathcal{L}(\Delta_p) = \frac{1}{1+\Delta_p^2}. \tag{18}$$

Substituting the above expression for the polarisation amplitude into (7) and (9) leads to the Class B laser model

$$\dot{E} = -(1+i\Delta_c)E + (1-i\Delta_p)\mathcal{L}(\Delta_p)NE + F(\tau), \tag{19}$$

$$\frac{1}{\gamma_{nc}}\dot{N} = \Lambda - N - \mathcal{L}(\Delta_p)|E|^2 N, \tag{20}$$

The above equations of motion are additionally invariant under the transformation

$$(E, F, \Delta_p, \Delta_c) \to (E^*, F^*, -\Delta_p, -\Delta_c). \tag{21}$$

The set of input parameters for which the rate equations (19) and (20) are valid is referred to as class B condition or limit.

III. THE SOLITARY CLASS C LASER

A solitary class C laser is described by Maxwell-Bloch equations (7)–(9) with $F(\tau) = 0$. It has two asymptotic solutions with constant $|E(\tau)|$ and $N(\tau)$: a non-lasing steady-state

$$\begin{aligned} E &= P = 0, \\ N &= \Lambda, \end{aligned} \tag{22}$$

and a lasing solution

$$|E_s|^2 = \Lambda - 1 - \Delta_p^2, \tag{23}$$
$$\varphi_s(\tau) = (\Delta_p + \Delta_c)\tau + \varphi_0, \tag{24}$$
$$P_s(\tau) = -(\Delta_p + i)|E_s|e^{-i[(\Delta_c+\Delta_p)\tau+\varphi_0]}, \tag{25}$$
$$N_s = 1 + \Delta_p^2, \tag{26}$$

where φ_0 is a constant that depends on initial phase $\varphi(0)$.

Suppose we choose ν to be the lasing frequency ν_s. From how the laser field is written in (1), such a choice is equivalent to having $d\varphi_s/dt = 0$, or according to (24), $\Delta_c = -\Delta_p$. The latter in turn gives the lasing frequency

$$\nu_s = \frac{\Omega\gamma_p + \omega\gamma_c}{\gamma_p + \gamma_c}. \tag{27}$$

The polarisation detuning parameter then becomes

$$\Delta_p^{(s)} := \Delta_p(\nu_s) = \frac{\omega - \nu_s}{\gamma_p} = \frac{\Omega - \omega}{\gamma_p + \gamma_c}, \tag{28}$$

and lasing solution (23)–(26) becomes a steady state given by

$$\begin{aligned} |E_s|^2 &= \Lambda - \frac{1}{\mathcal{L}(\Delta_p^{(s)})}, \\ \varphi_s &= \varphi_0, \\ P_s &= -(\Delta_p^{(s)} + i)|E_s|e^{-i\varphi_0}, \\ N_s &= \frac{1}{\mathcal{L}(\Delta_p^{(s)})}. \end{aligned} \tag{29}$$

Due to the rotational symmetry (21), there is a whole circle of lasing steady states parametrised by φ_0 in the (E, P, N) phase-space; this is known as phase indeterminacy of the laser field.

Both classes B and C conditions give the same steady state lasing solutions if we assume $\Delta_p^{(s)}$ is an input parameter. The difference lies away from steady state, that is in stability of steady-state solutions when subjected to perturbations. The analysis of laser stability may be approached from two perspectives: linear stability analysis and degree of dissipation.

Linear stability analysis is based on the characteristic equation or eigenvalues of the Jacobian of (7)–(9) evaluated at a steady state (22) or (29). It shows that non-lasing steady state (22) is stable if $\Lambda < 1 + (\Delta_p^{(s)})^2$. At the "laser first threshold", when $\Lambda = \Lambda_s^{thr} = 1 + (\Delta_p^{(s)})^2$, non-lasing steady-state destabilises via an infinite pitchfork bifurcation giving rise to a stable circle of lasing steady states as described by (29). A lasing steady state (29) has one eigenvalue that always equals zero (owing to the rotational symmetry) and four other eigenvalues which are solutions to a quartic characteristic equation,

$$0 = \lambda^4 + a_3\lambda^3 + a_2\lambda^2 + a_1\lambda + a_0, \tag{30}$$

where

$$\begin{aligned}
a_3 &= 2 + \gamma_{nc} + 2\gamma_{pc},\\
a_2 &= \left(\Delta_p^{(s)}\right)^2 (\gamma_{pc} - 1)^2 + (\gamma_{pc} + 1)^2 + \left(2 + (2 + |E_s|^2)\gamma_{pc}\right)\gamma_{nc},\\
a_1 &= \left[1 + \left(\Delta_p^{(s)}\right)^2 (\gamma_{pc} - 1)^2 + \left(2 + \gamma_{pc} + (3 + \gamma_{pc})|E_s|^2\right)\gamma_{pc}\right]\gamma_{nc},\\
a_0 &= 2(1 + \gamma_{pc})|E_s|^2\gamma_{pc}\gamma_{nc}.
\end{aligned}$$

We order the eigenvalues according to

$$\mathrm{Re}[\lambda_4] \le \mathrm{Re}[\lambda_3] \le \mathrm{Re}[\lambda_2] \le \mathrm{Re}[\lambda_1]. \tag{31}$$

In the 1980's [11,12], the stability of lasing steady state (29) was studied in relation to a "laser second threshold", where this state destabilises via Hopf bifurcation. This happens when two eigenvalues that are complex conjugate of each other cross the imaginary axis from left to right, i.e. when $\mathrm{Re}[\lambda_1] = \mathrm{Re}[\lambda_2] = 0$ and $\mathrm{Im}[\lambda_1] = -\mathrm{Im}[\lambda_2] \neq 0$. Hopf bifurcation may be found by assuming that quartic equation (30) has two pure imaginary roots, so that it has the form $(\lambda^2 + b^2)(\lambda^2 + b_1\lambda + b_0) = 0$. When cavity is tuned to transition resonance, i.e. $\Delta_p^{(s)} = 0$, and in the "bad cavity limit" $\gamma_c > \gamma_n + \gamma_p$, one obtains a simple condition for the "laser second threshold"

$$\Lambda = \Lambda_s^H = \frac{1 + \gamma_{nc} + 3\gamma_{pc}}{(1 - \gamma_{nc} - \gamma_{pc})\gamma_{pc}}. \tag{32}$$

When $\Delta_p^{(s)} \neq 0$, the analytical condition becomes rather complicated [31]. Since a laser second threshold cannot occur in the class B limit, one has a flagship example of the widely expected destabilising effects of class C conditions. However, we now show that such an association to only destabilisation with class C conditions is misleading.

Figure 1 illustrates that the transition from class B to class C conditions can make laser operation either less or more stable. We show the former with the parameter combination $(\Delta_p^{(s)}, \gamma_{nc}, \Lambda) = (0, 1, 3)$ and γ_{pc} decreasing from 20 in (a) to 1.5 in (b), and the latter with $(\Delta_p^{(s)}, \gamma_{nc}, \Lambda) = (2, 2, 6)$ and γ_{pc} decreasing from 20 in (c) to 2 in (d).

Laser stability is determined by the least damped solution under small perturbations, i.e. by eigenvalue(s) λ_n with the largest $\mathrm{Re}[\lambda_n]$ or with the lowest n according to the assignment in Eq. 31. In Fig. 1 the four non-zero eigenvalues for class C laser model, denoted with $\lambda_1, \lambda_2, \lambda_3$ and λ_4, are plotted with circles, and the two non-zero eigenvalues for class B laser model, denoted with λ_1^B and λ_2^B, are plotted with squares. We found by comparing results of class B and class C laser models that there is negligible difference in the predictions of the two models for $\gamma_p \gtrsim 20\gamma_c$. This is evidenced in Fig. 1 (a) and (c) for $\gamma_{pc} = 20$ and class B conditions, where the two least damped solutions in class C laser model are almost identical to the solutions of the class B model. Specifically, complex-conjugate eigenvalues in Fig. 1 (a) satisfy $\lambda_1 = \lambda_2^* \simeq \lambda_1^B = (\lambda_2^B)^*$, while real eigenvalues in Fig. 1 (b) satisfy $\lambda_1 \simeq \lambda_1^B$ and $\lambda_2 \simeq \lambda_2^B$. On the other hand, the two most damped solutions in class C laser model, with $\mathrm{Re}[\lambda_{3,4}]$ at least an order of magnitude greater than $\mathrm{Re}[\lambda_{1,2}]$, describe fast decay of the complex polarisation and justify its adiabatic elimination. As γ_{pc} decreases towards class C limit, λ_1 and λ_1 gradually deviate from λ_1^B and λ_1^B, respectively, and real parts of $\lambda_1, \lambda_2, \lambda_3$ and λ_4 become comparable. In Fig. 1 (b) for $\gamma_{pc} = 1.5$ and class C conditions, we found that the least damped solutions are two oscillatory ones in class C laser model with $\lambda_1 = \lambda_2^*$. As shown in the plot,

$\mathrm{Re}[\lambda_1] = \mathrm{Re}[\lambda_2] > \mathrm{Re}[\lambda_1^B] = \mathrm{Re}[\lambda_1^B]$, consistent with the general perception of transition from class B to class C conditions leading to lesser stability. The reason being that the system has greater degree of freedom without the adiabatic elimination of polarisation dynamics. However, in Fig. 1 (d) for $\gamma_{pc} = 2$ and class C conditions, we found solutions with $\lambda_1 < \lambda_1^B$. Here, one has an opposite and less intuitive trend where a laser becomes more stable when conditions change from class B to class C.

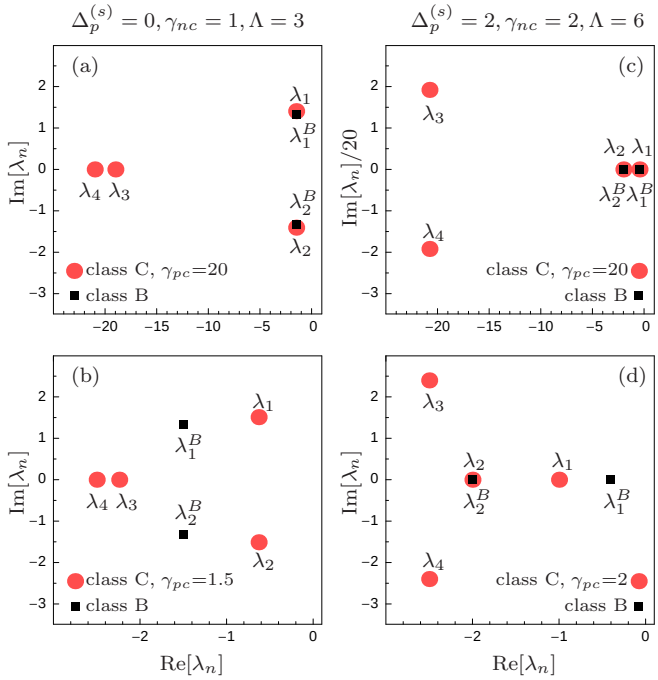

FIG. 1. Eigenvalue spectra of lasing steady state (29) for two sets of $(\Delta_p^{(s)}, \gamma_{nc}, \Lambda)$ in class B laser model (squares) and class C laser model (dots). In class C laser model, class B conditions are obtained using $\gamma_p = 20\gamma_c$ in (a) and (c), and class C conditions are obtained using $\gamma_p = 1.5\gamma_c$ in (b) and $\gamma_p = 2\gamma_c$ in (d).

To systematically study effects of class C conditions, which are intricately dependent on $\Delta_p^{(s)}$, γ_{nc} and Λ, we introduce a relative stability difference,

$$\zeta = \frac{\mathrm{Re}[\lambda_1^B(\Delta_p^{(s)}, \gamma_{nc}, \Lambda)] - \mathrm{Re}[\lambda_1(\Delta_p^{(s)}, \gamma_{nc}, \gamma_{pc}, \Lambda)]}{\mathrm{Re}[\lambda_1^B(\Delta_p^{(s)}, \gamma_{nc}, \Lambda)]}. \tag{33}$$

Heree, $\mathrm{Re}[\lambda_1(\Delta_p^{(s)}, \gamma_{nc}, \gamma_{pc}, \Lambda)]$ determines the actual laser stability (i.e., using the class C laser model) and

$$\lambda_1^B(\Delta_p^{(s)}, \gamma_{nc}, \Lambda) = -\frac{\gamma_{nc}\Lambda_{\mathcal{L}}}{2}\left(1 - \sqrt{1 - 8\frac{\Lambda_{\mathcal{L}} - 1}{\gamma_{nc}\Lambda_{\mathcal{L}}^2}}\right),$$

where $\Lambda_{\mathcal{L}} = \Lambda\mathcal{L}(\Delta_p^{(s)})$, determines the stability under class B conditions (i.e., using the class B laser model and the same input parameters). Positive (negative) relative stability difference indicates that the laser is less (more) stable than operating under class B conditions.

Figure 2 shows the relative stability difference (33) for lasing steady state (29) in terms of five differently patterned regions. The plots reveal several general and interesting features arising from the intermixing of regions of decreasing and increasing stability. First, as γ_{pc} decreases towards more pronounced class C conditions, the laser tends to eventually become less stable,

as indicated by the (hatched) dark regions, or more stable, as indicated by the hatched light regions. The exact stability changes depend on the chosen path as decided by Λ, γ_{nc} and $\Delta_p^{(s)}$.

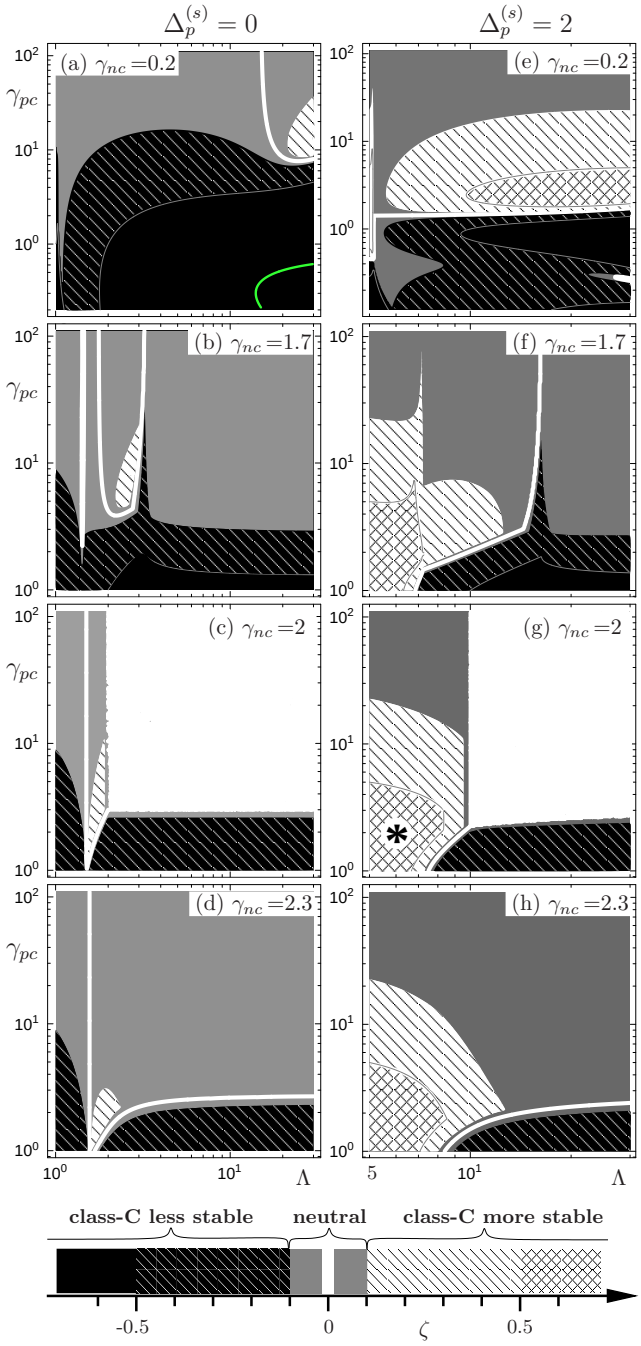

FIG. 2. Relative stability difference (33) for the lasing equilibrium (29) shown in the (Λ, γ_{pc}) plane for (top to bottom) increasing values of γ_{nc}, and for two values of $\Delta_p^{(s)}$ = (left column) 0 and (right column) 2. The green curve in (a) indicates "laser second threshold" where steady lasing destabilises via Hopf bifurcation. The asterisk in (g) indicates parameters used for the two examples of stabilising effects of class C conditions in the presence of external optical signals in Sec. IV and V.

The second feature involves polarisation detuning $\Delta_p^{(s)}$. For $\Delta_p^{(s)} = 0$ (left column, Fig. 2), where the cavity is tuned to the transition resonance, hatched light regions indicating stabilising tendency of class C conditions are appreciably smaller compared to (hatched) dark regions indicating destabilising tendency of class C conditions. By comparison, the stabilising

regions are noticeably larger for $\Delta_p^{(s)}= 2$ (right column, Fig. 2).

The third feature involves the case of equal cavity and population decay rates ($\gamma_{nc} = 2$). Starting with $\gamma_{nc} = 0.2$ and moving from top to bottom in Fig. 2, at first, the relative positions and shapes of the stabilising and destabilising regions in the (Λ, γ_{pc}) plane change continuously and gradually with increasing γ_{nc}. Then, these regions undergo a number of abrupt changes near $\gamma_{nc} = 2$, before becoming practically unchanged for $\gamma_{nc} \gtrsim 5$ (not plotted). The situation for $\gamma_{nc} = 2$ appears to be special, with a large white region of $\zeta = 0$ indicating exactly equal stability. The $\zeta = 0$ condition is described by a complicated surface in the three-dimensional $(\Lambda, \gamma_{pc}, \gamma_{nc})$ parameter space. Typical intersections between this surface and the plane of constant γ_{nc} shown in plots are smooth white curves. Interestingly, the surface appears to have a segment that lies exactly in the plane of $\gamma_{nc} = 2$, giving rise to a large white intersection region in panels (c) and (g). Finally, the absolute value of the relative stability difference remains below 0.1 when γ_{pc} is about one or two orders of magnitude larger than γ_{nc}, as indicated by the solid grey and white regions.

Lasing stability may also be analysed from the perspective of degree of dissipation. This quantity is defined as the rate of phase-space volume contraction and is related to the divergence of the laser vector field by the divergence theorem [33, Sec.1.4]. To see that, we rewrite Eqs. (7)–(9) and Eqs. (19)–(20) in the form

$$\dot{x} = G_C(x) \quad \text{and} \quad \dot{y} = G_B(y),$$

respectively, where $x = (E, P, N) \in \mathbb{R}^5$ is the laser vector state in class C laser model and $y = (E, N) \in \mathbb{R}^3$ is the laser vector state in class B laser model. In the equations, G_C and G_B denote the corresponding vector fields. Then, we find that

$$\nabla \cdot G_C = -2(1 + \gamma_{nc}/2 + \gamma_{pc}),$$

is independent of the laser state x, but

$$\nabla \cdot G_B = -2\left(1 - N\mathcal{L}\left(\Delta_p^{(s)}\right)\right) - \gamma_{nc}\left(1 + |E|^2\mathcal{L}\left(\Delta_p^{(s)}\right)\right),$$

depends on the laser state y.

TABLE I. Bifurcation labels.

S or S_l		local saddle-node bifurcation in which a pair of steady-amplitude solutions is born, where one is unstable and the other can be stable or unstable
S_g		global saddle-node bifurcation taking place on a limit cycle (periodic orbit),
H		Hopf bifurcation in which a steady-amplitude solution changes stability and gives rise to a solution with periodically modulated amplitude,
h		homoclinic bifurcation in which the period of a solution with periodically modulated amplitude reaches infinity and the solution disappears,
SL		saddle-node bifurcation of periodically modulated amplitude solutions,
A		non-central homoclinic bifurcation point,
B		generalised Hopf or Bautin bifurcation point,
BT		Bogdanov-Takens bifurcation point,
C		cusp bifurcation point,
D		resonant homoclinic bifurcation point.

Lately, a rich variety of instabilities and chaotic dynamics originating at saddle-node-Hopf bifurcations [32,25] have been reported, theoretically and experimentally, for *weakly dissipative* class B semiconductor lasers with external optical signals [**?**,23]. In those lasers, weak dissipation $\nabla \cdot G_B \sim -10^{-3}$ arises from $\gamma_{nc} \sim 10^{-3}$ and $N\mathcal{L}(\Delta_p^{(s)}) \approx 1$. This paper gives examples of stability diagrams for *dissipative* lasers. More specifically, we use $\gamma_{nc} = 2$ so that $\nabla \cdot G_B \sim -1$ and less instabilities are expected.

The next two sections provide general analysis of class C laser response to optical injection and time-delayed feedback. In particular, they illustrate the less intuitive stabilising effects of class C conditions for laser parameters indicated by the asterisk in Fig. 2 (g). The results are presented in terms of bifurcation or stability diagrams, which include various bifurcations (instabilities) described in Table I. In the diagrams, solid curves denote bifurcations of stable solutions that can be directly observed in laser experiments while dashed curves denote bifurcations of unstable solutions. For more details on bifurcation theory we refer to [34].

IV. EXTERNAL OPTICAL INJECTION

An optically-injected class C laser can be modelled by Maxwell-Bloch equations (7)–(9) with $F(\tau)$ describing the injected field [30]. We consider a weak monochromatic injected field of magnitude $|\mathcal{E}_{ext}|$, so that

$$F(\tau) = \eta_i \, \exp\left(-i(\nu_i - \nu)\tau/\gamma_c\right) = \frac{c\,|\mathcal{E}_{ext}|}{2nL\mathcal{E}_0\gamma_c}\sqrt{\frac{T}{1-T}}\, \exp\left(-i(\nu_i - \nu)\tau/\gamma_c\right),$$

where η_i is a normalised *injection rate*, ν_i is the injected light frequency, c is the speed of light, n is the background refractive index, L is the cavity length and T is the transmission coefficient for injected field. We are interested in 1:1 phase-locked solutions which correspond to the laser oscillating at the frequency of the externally injected signal. To study phase-locked solutions as steady states, we choose for this section

$$\nu = \nu_i,$$

in expansion (1), and introduce the *injection detuning* parameter

$$\Delta_i = \frac{\nu_i - \nu_s}{\gamma_c}.$$

This leads to

$$\Delta_c(\nu_i) = -\Delta_p^{(s)} - \Delta_i$$

and

$$\Delta_p(\nu_i) = \Delta_p^{(s)} - \frac{\Delta_i}{\gamma_{pc}}. \tag{34}$$

The above expression for $\Delta_p(\nu_i)$ reveals that, in contrast to class B conditions, the polarisation detuning in externally injected class C lasers varies with Δ_i and can be noticeably different from its solitary value if $\Delta_i \neq 0$. Then, (7)–(9) become

$$\dot{E} = -\left[1 - i(\Delta_p^{(s)} + \Delta_i)\right] E + iP + \eta_i, \tag{35}$$

$$\frac{1}{\gamma_{pc}}\,\dot{P} = -\left[1 + i\left(\Delta_p^{(s)} - \frac{\Delta_i}{\gamma_{pc}}\right)\right] P - iEN, \tag{36}$$

$$\frac{1}{\gamma_{nc}}\,\dot{N} = \Lambda - N - \frac{i}{2}\left(E^*P - EP^*\right). \tag{37}$$

Setting time derivatives in (35)–(37) to zero gives a cubic equation for the steady-state population inversion N_i:

$$0 = N_i^3 + c_2 N_i^2 + c_1 N_i + c_0, \tag{38}$$

where

$$\begin{aligned}
c_2 &= -\Lambda - 2\left[1 + \left(\Delta_p^{(s)} + \Delta_i\right)\left(\Delta_p^{(s)} - \frac{\Delta_i}{\gamma_{pc}}\right)\right], \\
c_1 &= 2\Lambda\left[1 + \left(\Delta_p^{(s)} + \Delta_i\right)\left(\Delta_p^{(s)} - \frac{\Delta_i}{\gamma_{pc}}\right)\right] + \frac{1 + \left(\Delta_p^{(s)} + \Delta_i\right)^2}{\mathcal{L}(\Delta_i)} + \eta_i^2, \\
c_0 &= -\Lambda\frac{1 + \left(\Delta_p^{(s)} + \Delta_i\right)^2}{\mathcal{L}(\Delta_i)},
\end{aligned}$$

and effects of class C conditions are represented by the term Δ_i/γ_{pc}, which also appears in the dimensionless Lorentzian

$$\mathcal{L}(\Delta_i) = \frac{1}{1 + \left(\Delta_p^{(s)} - \Delta_i/\gamma_{pc}\right)^2}.$$

The steady-state amplitude $|E_i|$ and the phase difference $\phi_i = \arg(E_i)$ between the injected and the laser fields are given by

$$|E_i| = \sqrt{\frac{\Lambda - N_i}{N_i\mathcal{L}(\Delta_i)}}, \tag{39}$$

$$\phi_i = \cos^{-1}\left(\frac{|E_i|}{\eta_i}\left[1 - N_i\mathcal{L}(\Delta_i)\right]\right). \tag{40}$$

The steady-state polarisation is given by

$$P_i = -\left(\Delta_p^{(s)} - \frac{\Delta_i}{\gamma_{pc}} + i\right)|E_i|N_i\mathcal{L}(\Delta_i)e^{-i\phi_i}.$$

It is clear from (36) that the steady-state solutions are independent of γ_{pc} when $\Delta_i = 0$. However, stability of these solutions will in general depend on γ_{pc} regardless of Δ_i.

Examples of lasing steady-state solutions in the presence of an injected field for class C and class B conditions are shown in Fig. 3. Plotted is the normalised laser intensity versus the normalised injection rate, for two combinations of $(\Delta_p^{(s)}, \Lambda)$. For small η_i and $\Delta_i \neq 0$, there is one unstable steady state (dashed portion of curves). Then for increasing η_i, two new steady states may be born and then disappear via saddle-node bifurcations. Where three steady states exist, the low-intensity one is always unstable, the high-intensity one is always stable, and the mid-intensity one can be either stable or unstable. The situation of bistable solutions is illustrated very well by the two curves in Fig. 3 (b).

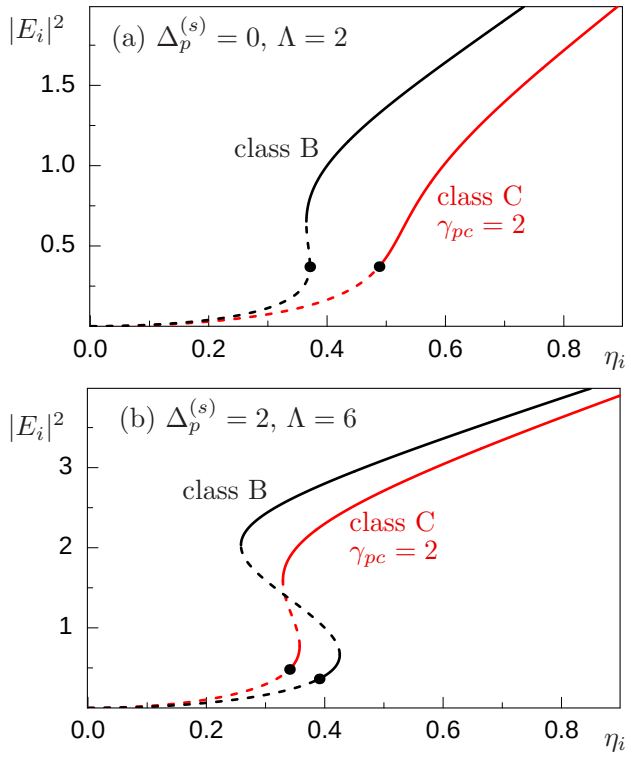

FIG. 3. Steady states (39) of an injected laser vs. the injection rate η_i for class B and class C conditions, with $\Delta_i = -0.4$, $\gamma_{nc} = 2$ and two sets of $(\Delta_p^{(s)}, \Lambda)$. Class B conditions are obtained using class B laser model, and class C conditions are obtained using class C laser model with $\gamma_{pc} = 2$. Solid curves denote stable steady states, dashed curves denote unstable steady states, and dots denote Hopf bifurcations.

Saddle-node bifurcations occur when the polynomial in (38) has a double root N_i, meaning that its first derivative with respect to N_i also equals zero, giving

$$N_i = -\frac{1}{3}\left(c_2 \pm \sqrt{c_2^2 - 3c_1}\right).$$

Inserting the above expression into (38) gives condition for saddle-node bifurcations in terms of input parameters only. Furthermore, the polynomial in (38) can have a triple root, corresponding to a cusp bifurcation, when its first and second derivatives are equal to zero. This occurs when

$$N_i = -c_2/3.$$

Inserting the above expression into (38) gives condition for cusp bifurcations in terms of input parameters only. When $\gamma_{pc} \to \infty$, we recover results derived for class B conditions in [32].

Figure 4 shows saddle-node bifurcation curves S and cusp bifurcation points C in the (η_i, Δ_i) parameter plane obtained from the derived formulae. All other bifurcations are computed using numerical bifurcation continuation software [35]. A solid (super-critical) part of S gives rise to a stable steady state. Furthermore, S_l refers to a local (regular) saddle-node bifurcation and S_g refers to a global saddle-node bifurcation taking place on a limit cycle [**?**]. Recall that limit cycles represent lasing solutions with periodically modulated amplitude. Transitions between S_l and S_g occur at non-central homoclinic bifurcation points A, from which a curve of homoclinic bifurcation h emerges. Along h, the period of the limit cycle involved goes to infinity and the cycle disappears.

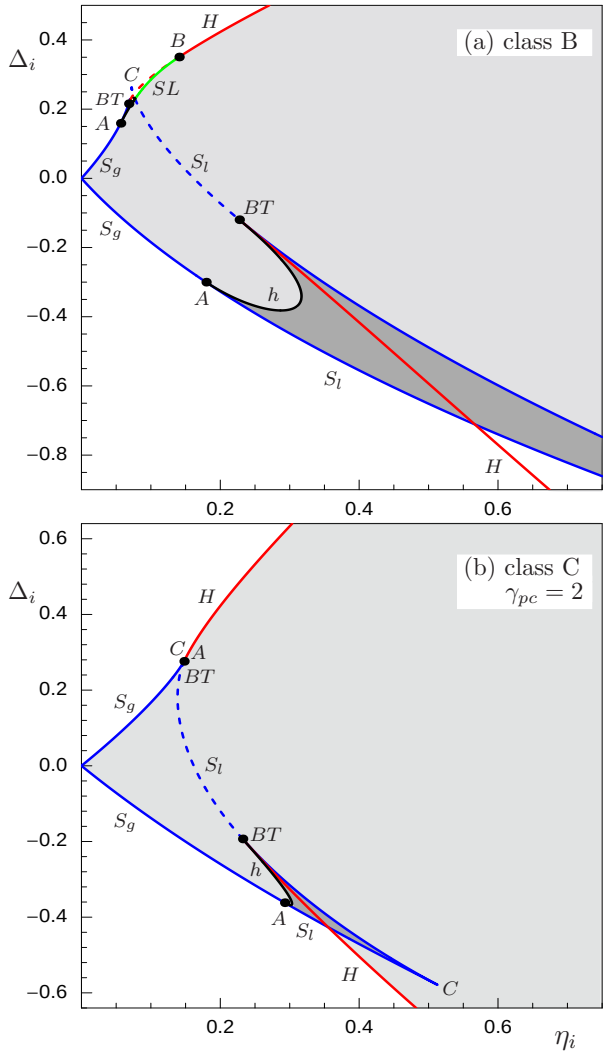

FIG. 4. Complete stability diagrams in the (η_i, Δ_i) plane for (a) class B and (b) class C conditions, with $\gamma_{nc} = 2$ and $\Delta_p^{(s)} = 2$. Class B conditions are obtained using class B laser model, and class C conditions are obtained using class C laser model with $\gamma_{pc} = 2$. Bifurcation curves define boundaries of (light and dark shading) 1:1 phase locking and (dark shading) bistability. Refer to Table I for bifurcation labels.

Homoclinic bifurcation curves reconnect to S at Bogdanov-Takens points BT which, in turn, give rise to a curve of Hopf bifurcation H. Typically, along H, a steady state changes stability and gives rise to a limit cycle. The cycle is stable only along the solid super-critical parts of S. In addition to typical behaviour, there can be special points on H called the generalised Hopf or Bautin points B, where H changes from super-critical to sub-critical. From these points a bifurcation curve of saddle-node of limit cycles SL emerges (figures 4(b) and 5). Finally, SL terminates on h at the resonant homoclinic bifurcation point D (figure 5).

Complete bifurcation diagrams in Figs. 4–5 include all instabilities that can be found for the chosen laser parameters. They explain how different instabilities are connected via special bifurcation points, of which Bogdanov-Takens points can be identified as the *organising centres* for dynamics. Most importantly, different bifurcations form boundaries of stable phase locking, periodic amplitude oscillations, and bistability. Note that, owing to strong dissipation, we have not found any instabilities leading to dynamics more complicated than periodic amplitude oscillations.

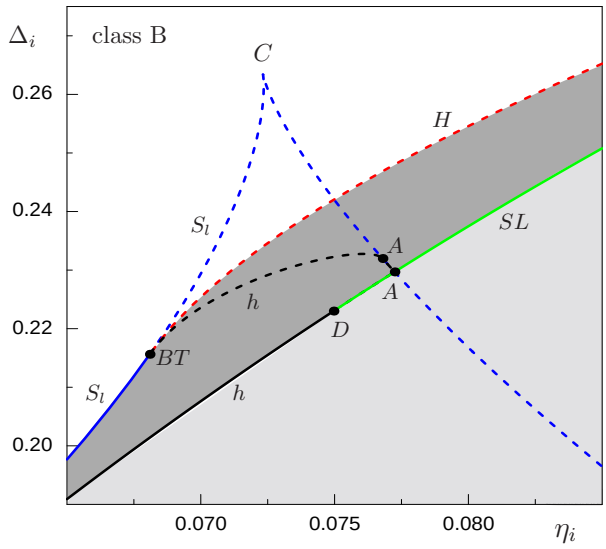

FIG. 5. An expanded view about the upper BT point from figure 4(a).

Shading in figure 4 indicates the region of stable 1:1 phase locking, with lighter shading indicating monostability and darker shading indicating bistability. Each panel in Fig. 4 has two bistability regions, one near each BT point. (Note that the smaller regions can be difficult to locate. For example, see the not discernable bistable region in the upper left quadrant of Fig. 4(b), which is expanded in Fig. 5.) To illustrate the origin of this bistability, we fix $\Delta_i = -0.4$ in Fig. 4(b) and increase η_i. At small η_i, the only stable state is a limit cycle corresponding to an unlocked lasing solution. When S_l is reached, a stable steady state is born (see also folds in Fig. 3), giving rise to bistability between phase-locked and phase-unlocked solutions. Then, the limit cycle shrinks onto an unstable steady state at H (see also dots in Fig. 3). This state in turn becomes stable, giving rise to bistability between two phase-locked solutions. Finally, the two steady states with the lowest field amplitude disappear at the other branch of S_l, leaving just one stable steady state.

It is clear from Fig. 4 that transition from class B to class C conditions can have a strong effect on both the symmetry of the locking region and the extent of bistability regions. The diagram in Fig. 4 (a) is reminiscent of what is usually found for class B conditions with $\Delta_p^{(s)} = 2$. The two key features are: strong asymmetry with respect to $\Delta_i = 0$ and a large region of bistability for $\Delta_i < 0$ [**?**].

When class C conditions are approached (Fig. 4(b)), the large bistability region shrinks noticeably and SL and B bifurcations disappear altogether. Moreover, the diagram becomes more symmetric, similar to the situation for class B conditions with $\Delta_p^{(s)} \approx 0$. However, the more symmetric shape of the locking region is not because of small $\Delta_p^{(s)}$. Rather, it is partially due to the fact that under class C conditions the polarisation detuning in an injected laser, that is $\Delta_p(\nu_i)$ given by (34), may differ from its solitary laser value. In particular, even if $\Delta_p^{(s)} > 0$, $\Delta_p(\nu_i)$ could become zero or even negative if Δ_i/γ_{pc} exceeds $\Delta_p^{(s)}$.

Overall, stability diagrams for an injected laser in Fig. 4 are in line with the stability analysis for a solitary laser. For the less stable class B conditions in Fig. 4(a), the laser has a large region of bistability and various instabilities. For the more stable class C conditions in Fig. 4(b), the region of bistability shrinks noticeably and certain instabilities, namely saddle-node of limit cycles SL and Bautin points B, disappear from the stability diagram.

V. OPTICAL FEEDBACK

A class C laser subjected to optical feedback can be modelled by Maxwell-Bloch equations (7)–(9) with $F(\tau)$ describing optical signal that is returned to the laser with a normalised *delay time* τ_f [36]:

$$F(\tau) = \eta_f e^{i\phi_f} E(\tau - \tau_f) = \frac{cT}{2nL\gamma_c}\sqrt{\frac{R_{ext}}{1-T}}\sqrt{1-\sigma}\; e^{i\phi_f} E(\tau - \tau_f),$$

where η_f is a normalised *feedback rate*, $\phi_f = \nu\tau_f/\gamma_c$ is the *feedback phase*, R_{ext} is the reflection coefficient of the external mirror and σ is the fraction of the light intensity that is lost in the feedback loop (e.g. owing to light absorption and diffraction of the laser beam). In this section we choose

$$\nu = \nu_s,$$

by setting $\Delta_c = -\Delta_p^{(s)}$. Due to the rotational symmetry of the Maxwell-Bloch equations, the simplest lasing solutions are circular limit cycles, also known as *rotating waves* (RWs):

$$\begin{aligned} E(\tau) &= |E_f| \exp\left(-i\Delta_f\tau\right), \\ P(\tau) &= P_f \exp\left(-i\Delta_f\tau\right), \\ N(\tau) &= N_f, \end{aligned} \tag{41}$$

where

$$\Delta_f = \frac{\nu_f - \nu_s}{\gamma_c},$$

is the normalised detuning between the RW frequency and the steady-state solitary-laser frequency, ν_f and ν_s, respectively.

Substituting (41) into (7)–(9) and setting $\Delta_c = -\Delta_p^{(s)}$, gives the transcendental equation for Δ_f:

$$\Delta_f + \eta_f\left[\Delta_p^{(s)}\cos(\phi_f + \Delta_f\tau_f) + \sin(\phi_f + \Delta_f\tau_f)\right] + \frac{\Delta_f}{\gamma_{pc}}\left[1 - \eta\cos(\phi_f + \Delta_f\tau_f)\right] = 0. \tag{42}$$

Furthermore, we derive

$$N_f = \frac{1}{\mathcal{L}\left(\Delta_f\right)}(1 - \eta\cos(\phi_f + \Delta_f\tau_f)), \tag{43}$$

$$|E_f|^2 = \frac{\Lambda - N_f}{N_f\mathcal{L}\left(\Delta_f\right)}, \tag{44}$$

$$P_f = -\left(\Delta_p^{(s)} - \frac{\Delta_f}{\gamma_{pc}} + i\right)|E_f|N_f\mathcal{L}\left(\Delta_f\right), \tag{45}$$

in terms of the dimensionless Lorentzian

$$\mathcal{L}(\Delta_f) = \frac{1}{1 + \left(\Delta_p^{(s)} - \Delta_f/\gamma_{pc}\right)^2}.$$

Note from (43)–(44) that a root Δ_f of (42) corresponds to a physical lasing solution only if the corresponding threshold condition is satisfied

$$\Lambda > \Lambda_f^{thr} := \frac{1 - \eta_f\cos(\phi_f + \Delta_f\tau_f)}{\mathcal{L}\left(\Delta_f\right)}.$$

For small η_f there is just one RW. Additional RWs are born typically in saddle-node bifurcations and are often called *external cavity modes*. Examples of RWs in the (Δ_f, N_f) plane with $\eta_f = 0.01$ are shown as dots in Fig. 6 for class B and class C conditions. As ϕ_f is varied, RWs are born in pairs via saddle-node bifurcations at an intersection point between the solid and dashed curves. One RW is always unstable and the other may be stable or unstable. Each RW traces out the solid curve, and then disappears into a different pair at the other intersection point between the solid and dashed curves. Saddle-node bifurcations occur when (42) has a double root, which corresponds to the vanishing of the first derivative of (42) with respect to Δ_f:

$$1 + \tau_f \eta_f \left[\cos(\phi_f + \Delta_f \tau_f) - \Delta_p^{(s)} \sin(\phi_f + \Delta_f \tau_f)\right] + \frac{1}{\gamma_{pc}} \left[1 - \eta_f \cos(\phi_f + \Delta_f \tau_f) + \Delta_f \tau_f \eta_f \sin(\phi_f + \Delta_f \tau_f)\right] = 0. \tag{46}$$

To illustrate the saddle-node condition (46) in the (Δ_f, N_f) plane, we first use (43) to express $\eta_f \cos(\phi_f + \Delta_f \tau_f)$ in terms of N_f. We then use the result and (42) to express $\eta_f \sin(\phi_f + \Delta_f \tau_f)$ in terms of N_f. Substituting both expressions into (46) gives

$$N_f \mathcal{L}(\Delta_f) = \frac{1 + \left(\Delta_p^{(s)}\right)^2 + \Delta_p^{(s)} \Delta_f + 1/\tau_f - \Delta_f \left(\Delta_p^{(s)} + \Delta_f\right)/\gamma_{pc}}{1 + \left(\Delta_p^{(s)}\right)^2 - \left[\Delta_f \left(2\Delta_p^{(s)} - \Delta_f/\gamma_{pc}\right) + 1/\tau_f\right]/\gamma_{pc}}. \tag{47}$$

For class B conditions, (47) reduces to a straight line

$$N_f \mathcal{L}(\Delta_p^{(s)}) = 1 + \frac{\Delta_p^{(s)} \Delta_f + 1/\tau_f}{1 + \left(\Delta_p^{(s)}\right)^2}. \tag{48}$$

The above saddle-node condition is plotted in Fig. 6 as dashed curves, where class C conditions are obtained using (47) with $\gamma_{pc} = 2$, and class B conditions are obtained using (48). Furthermore, (42) can have a triple root, corresponding to a cusp bifurcation, when the second derivative of (42) with respect to Δ_f also vanishes:

$$\tau_f^2 \eta_f \left[\sin(\phi_f + \Delta_f \tau_f) + \Delta_p^{(s)} \cos(\phi_f + \Delta_f \tau_f)\right] - \frac{\tau_f \eta_f}{\gamma_{pc}} \left[2 \sin(\phi_f + \Delta_f \tau_f) + \Delta_f \tau_f \cos(\phi_f + \Delta_f \tau_f)\right] = 0. \tag{49}$$

In (42)–(49), class C effects are represented by terms with the factor $1/\gamma_{pc}$. When $\gamma_{pc} \to \infty$, we recover results derived for class B conditions in [25].

Figure 6 highlights stabilising effects of class C conditions on the structure and number of RWs. Firstly, as γ_{pc} decreases towards class C conditions, the number of RWs decreases. Secondly, while the RWs still trace out an ellipse in the (Δ_f, N_f) plane, the slope of its major axis becomes more horizontal, and the ellipse becomes less (more) circular when $\Delta_p^{(s)} = 0$ ($\Delta_p^{(s)} > 0$).

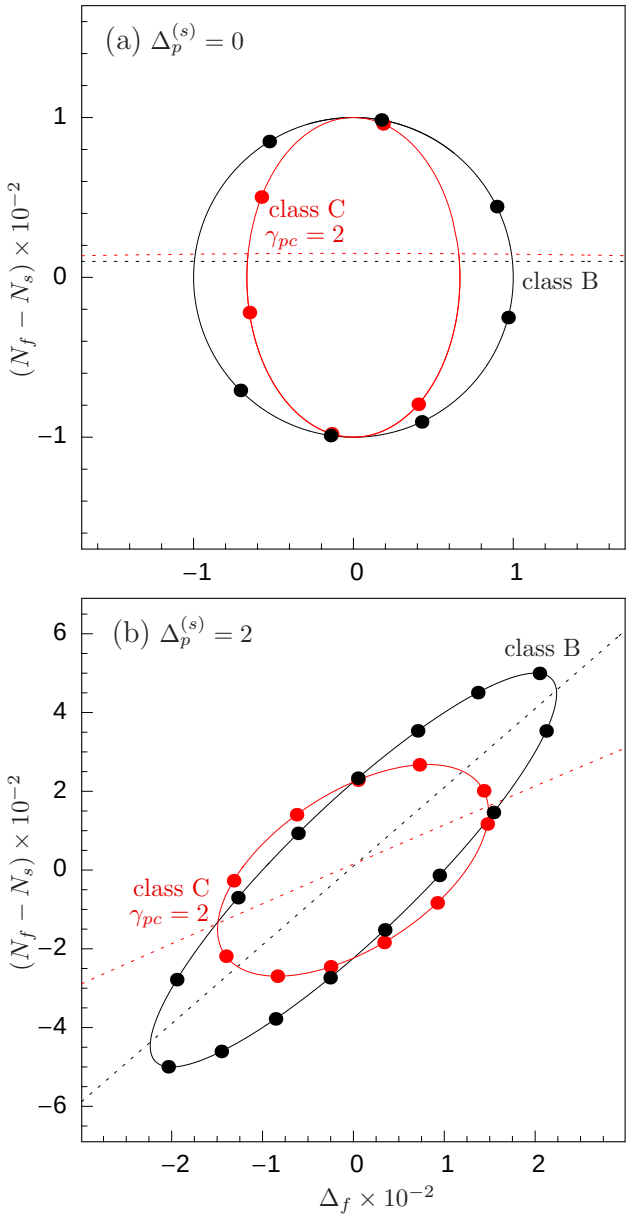

FIG. 6. (Dots) Rotating waves or external cavity modes (41) in the (Δ_f, N_f) plane for class B and class C conditions, with $\tau_f = 10^3$ corresponding to a feedback-loop length of $3 \times 10^{11}/\gamma_c$ m, $\eta_f = 0.01$, $\gamma_{nc} = 2$, and two values of $\Delta_p^{(s)} =$ (a) 0 and (b) 2. Class B conditions are obtained using class B laser model, and class C conditions are obtained using class C laser model with $\gamma_{pc} = 2$. Solid curves are the paths traced out by the dots when the feedback phase ϕ_f is varied. Rotating waves are born and disappear in pairs via saddle-node bifurcations at the intersections of solid and dashed curves.

In Fig. 7(a), we plotted saddle-node bifurcation curves S using (46) and cusp bifurcation points C using (49) in the (ϕ_f, η_f) plane. The resulting bifurcation structure is 2π-periodic in ϕ_f, which follows from (46). Two additional RWs are born when each branch of saddle-node curve S is crossed in the direction of increasing η_f. Different digits indicate the number of RWs in different regions of the plane. Numerical stability analysis [37] reveals that within a region with n coexisting RWs, a maximum possible number of $(n+1)/2$ RWs are stable. This means that the bifurcation diagram in Fig. 7 has a high degree of RW multistability (shading) but is devoid of any field-amplitude instabilities. In other words, there are no solutions with oscillating field amplitude that bifurcate from RWs.

Figure 7(b) shows stabilising effects of class C conditions in the stability diagram. For clarity, we plotted just one S curve for class C conditions and one S curve for class B conditions. The main effect is that, as γ_{pc} decreases towards class C conditions, the cusp points move towards higher η_f. This implies that for a fixed η_f the number of RWs decreases with decreasing γ_{pc} in agreement with Fig. 6. Again, numerical stability analysis confirms that RWs associated with the plotted saddle-node bifurcation curves do not undergo any instabilities within the range of η_f and ϕ_f shown in the figure.

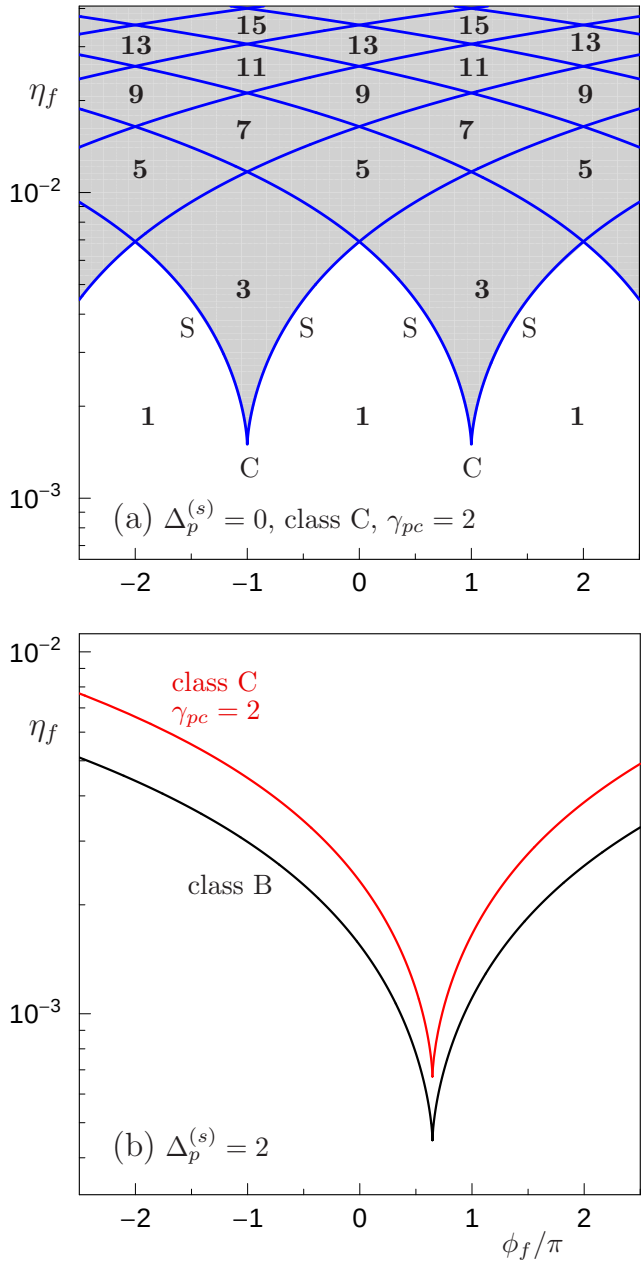

FIG. 7. (a) Complete stability diagram in the (ϕ_f, η_f) plane showing saddle-node bifurcation curves S and cusp bifurcation points C of rotating waves or external cavity modes (41) for class C conditions obtained using class C laser model with $\gamma_{pc} = 2$, $\Delta_p^{(s)} = 0$ and $\Lambda = 2$. Digits indicate the number n of coexisting rotating waves, where $(n+1)/2$ are stable. Shading indicates multistability. (b) Effect of transition from class B to class C conditions on the saddle-node bifurcations for $\Delta_p^{(s)} s = 2$ and $\Lambda = 6$. The class B saddle-node curve was obtained using class B laser model and class C saddle-node curve was obtained using class C laser model with $\gamma_{pc} = 2$. In (a) and (b) we used $\gamma_{nc} = 2$ and $\tau_f = 10^3$.

In view of the relatively simple bifurcation diagrams in Fig. 7, a question arises about the possibility of field-amplitude instabilities in dissipative lasers with $\gamma_{nc} = 2$. Figure 8, obtained using direct time integration of (7)–(9) with $\eta_f = 4 \times 10^{-2}$ and $\Lambda = 5.2$, demonstrates that such instabilities do occur but they require a strong feedback rate and operation in close proximity to the lasing threshold. Specifically, complex nonlinear dynamics is observed for class B conditions in Fig. 8(a). Starting from $\phi_f = 0$, the laser converges to a complicated (possibly chaotic) attractor and produces irregular field-amplitude oscillations whose extrema appear to form a recurring pattern in ϕ_f. Next, for $\phi_f \approx 8\pi$, the laser leaves the chaotic state and converges to a branch of RWs. It follows this branch up to $\phi_f \approx 16\pi$, then converges to another branch of RWs. Hence, the laser remains on stable branches of RWs as ϕ_f increases. On the other hand, as ϕ_f decreases below zero (not shown), the laser continues to produce irregular oscillations without any transitions to RWs. Numerical bifurcation analysis using [37] reveals that the branch of RWs in Fig. 8(a) that exists on the interval $\phi_f/\pi \in [-41.3, 16.6]$ is stable for $\phi_f/\pi \in [-7.7, 16.4]$. It looses stability via Hopf bifurcations at $\phi_f/\pi \approx -7.7$ and 16.4.

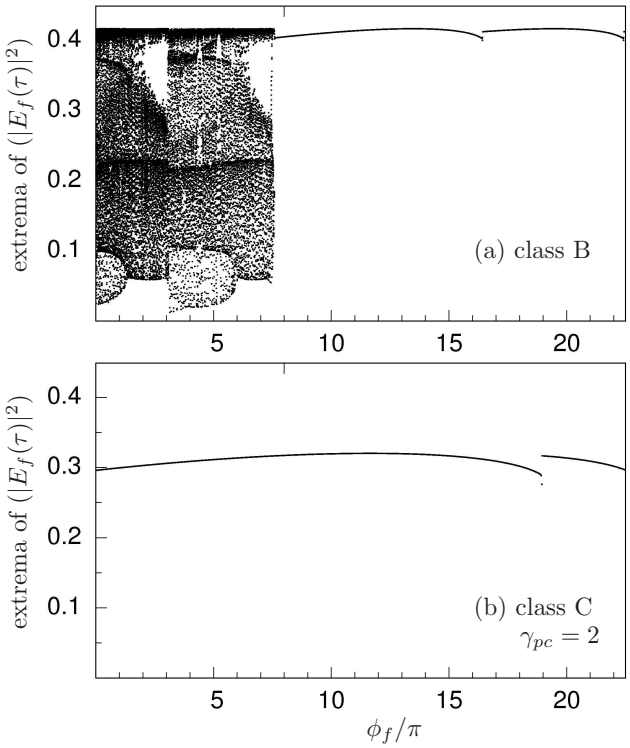

FIG. 8. One-dimensional attractor diagrams showing extrema of $|E_f(\tau)|^2$ vs. the feedback phase ϕ_f for (a) class B conditions obtained using class B laser model and (b) class C conditions obtained using class C laser model with $\gamma_{pc} = 2$. In (a) and (b) we used $\eta_f = 0,04$, $\tau_f = 10^3$, $\gamma_{nc} = 2$, $\Delta_p^{(s)} = 2$, $\Lambda = 5.2$, and we initialised the system identically near the non-lasing steady-state of a solitary laser.

A rather different bifurcation transition is observed for class C conditions in Fig. 8(b). Branches of stable RWs span over a large interval of ϕ_f, indicating a high degree of multi-stability. Furthermore, there is no evidence of any amplitude-field oscillations. Starting from $\phi_f = 0$, the laser converges to a branch of RWs. However, it leaves this primary branch of RWs and converges to another branch of RWs before the primary branch disappears in a saddle-node bifurcation. This means that RWs destabilise before they disappear. For example, the first branch in Fig. 8(b) exists on the interval $\phi_f/\pi \in [-19.6, 19.4]$ but the laser stays on this branch for $\phi_f/\pi \in [-15.2, 18.9]$. More accurate numerical bifurcation analysis using [37] uncovers sub-critical Hopf bifurcations, which destabilise this branch at $\phi_f/\pi \approx -15.2$ and 18.9. Since

periodic orbits involved in sub-critical Hopf bifurcations are unstable, we do not observe any field-amplitude oscillations in Fig. 8(b). Rather, the laser converges to a nearby stable RW.

In summary, stability and attractor diagrams for a laser with optical feedback are in line with the stability analysis of a solitary laser. The laser undergoes instabilities leading to irregular field-amplitude oscillations for the less stable class B conditions in Fig. 8(a), but not for the more stable class C conditions in Fig. 8(b).

VI. CONCLUSIONS

Owing to the recent developments of novel laser systems, there is renewing interest in questions pertaining to laser stability during the transition between class B and class C conditions. The former, which apply to almost all semiconductor lasers, occurs when active-medium polarisation dynamics is sufficiently fast to allow its adiabatic elimination from the laser equations. The latter occurs when laser-field, population inversion and polarisation dynamics evolve on similar timescales and laser description has to be via the full set of Maxwell-Bloch equations. Earlier studies of laser dynamics under class C conditions led to specific examples of destabilisation under class C conditions. A well-known situation led to the classic phenomenon of "laser second threshold".

This paper extends those studies by performing a systematic investigation aimed at achieving a general and comprehensive understanding of the transition from class B to class C dynamics. The investigation is based on the Maxwell-Bloch laser equations and the calculations demonstrate that under a broader range of class C conditions, polarisation dynamics can have either stabilising or destabilising influences on laser operation. Combinations of the ratio of field and population decay rates, excitation rate and detunings between cavity and transition frequencies or injected signal and free-running laser frequencies leading to these two opposite effects were identified.

In situations involving the less intuitive stabilising effects of class C conditions, the enabling mechanism is found to be the decrease in the number of coexisting lasing solutions. The consequence is greater stability of the steady-state lasing solutions by partial or even complete suppression of any externally-induced instabilities and ensuing field-amplitude oscillations. The lasers configurations studied involve external optical injection and time-delayed optical feedback.

In the case of optical injection, an example is considered where the stability diagram under class B conditions has a large region of bistability, as well as homoclinic and saddle-node bifurcations giving rise to periodic amplitude oscillations. When approaching class C conditions, the bistability region shrinks noticeably and some bifurcations leading to stable field-amplitude oscillations disappear. Simultaneously, the phase-locked region becomes more symmetric with respect to positive and negative detuning between injected and free-running frequencies.

In the case of optical feedback, we considered an example where the stability diagram for class B conditions consists of rotating wave instabilities and highly irregular (possibly chaotic) field-amplitude oscillations. When approaching class C conditions, the number of rotating wave solutions decreases. Moreover, all regular and irregular field-amplitude oscillations disappear. The resulting stability diagram for class C conditions is highly multistable but devoid of any rotating wave instabilities that could lead to stable field-amplitude oscillations.

[1] S. Wieczorek, B. Krauskopf, T. B. Simpson, and D. Lenstra, *Physics Reports*, **416** (1–2) 1–128 (2005)
[2] S. Wieczorek and W. W. Chow, *Optics Communications*, **282** (12) 2367–2379 (2009)
[3] S. Tang and J.M. Liu, *IEEE Quant. Electron.*, **37** (3) 329–336 (2001)
[4] T.Heil, I. Fisher, W. Elsässer, J. Mulet and C.R. Mirasso, "Chaos Synchronization and Spontaneous Symmetry-Breaking in Symmetrically Delay-Coupled Semiconductor Lasers" *Phys. Rev. Lett* **86** 795–798 (2001)
[5] S.Wieczorek and W.W. Chow, *Phys. Rev. A* **69** 033811 (2004)
[6] S. Wieczorek and W.W. Chow, *Phys. Rev. Lett.* **92** 213901 (2004)
[7] F. Rogister and R. Roy, *Phys. Rev. Lett.*, **98** 104101 (2007)
[8] M. Sargent III, M.O. Scully, and W.E. Lamb Jr., *Laser Physics*, Addison-Wesley, 1974.
[9] Special issue on Instabilities in Active Optical Media, *J. Opt. Soc. Am. B* **2**, (1985).
[10] H. Haken, *Laser Light Dynamics, Vol II*, Elsevier Science Publishers B.V., Amsterdam 1985.
[11] C.O. Weiss and R. Vilaseca, *Dynamics of lasers*, VCH Verlagsgesellschaft, Weinheim, Germany 1991.
[12] P. Mandel, *Theoretical Problems in Cavity Nonlinear Optics*, Cambridge University Press 1997.
[13] B. Krauskopf and D. Lenstra (Eds.), *Fundamental Issues of Nonlinear Laser Dynamics*, AIP Conference Proceedings **548** 2000.
[14] D.M. Kane and K.A. Shore (Eds.), *Unlocking Dynamical Diversity: Optical Feedback Effects on Semiconductor Lasers*, John Wiley & Sons 2005.
[15] K. Ludge (Ed.), *Nonlinear Laser Dynamics - From Quantum Dots to Cryptography*, Wiley-VCH Verlag 2012.
[16] G. VanWiggeren and R. Roy, *Science*, **279** (5354) 1198–1200 (1998)
[17] S. Wieczorek, W. W. Chow, L. Chrostowski, and C. J. Chang-Hasnain, *IEEE J. of Quant. Electron.*, **42** (6) 552–562 (2006)
[18] L. Chrostowski, B. Faraji, W. Hoffmann, M.C. Amann, S. Wieczorek and W. W. Chow, *IEEE J. of Selected Topics in Quant. Electron.*, **13** (5) 1200–1208 (2007)
[19] J.V. Moloney, J.S. Uppal, and R.G. Harrison, *Phys. Rev. Lett.*, **59** (25) 2868–2871 (1986)
[20] S. Wieczorek and W. W. Chow, *Phys. Rev. Lett.*, **97** 113903 (2006)
[21] A. Uchida1, K. Amano1, M. Inoue, K. Hirano, S. Naito, H. Someya, I. Oowada, T. Kurashige, M. Shiki, S. Yoshimori, K. Yoshimura and P. Davis, *Nature Photonics*, **2** 728–732 (2008)
[22] W.W. Chow and S. Wieczorek, *Optics Express*, **17** (9) 036209 7491–7504 (2009)
[23] M.C. Soriano, J. Garcia-Ojalvo, C.R. Mirasso and I. Fischer, *Rev. Mod. Phys.*, **8**5, 421-470 (2013).
[24] S. Wieczorek in: B. Krauskopf, H.M. Osinga and J. Galan-Vioque (Eds.), *Numerical Continuation Methods for Dynamical Systems: Path following and boundary value problems*, Chapter 6, , Springer-Verlag (2007), 177-220.
[25] M. Wolfrum and D. Turaev, *Opt. Comm.*, **2**12, 127-138 (2002).
[26] F.T. Arecchi, G. Lippi, G. Puccioni, J. Tredicce, in: L. Mandel and E. Wolf (Eds.), *Coherence and Quantum Optics V*, Plenum, New York, 1984.
[27] G.P. Agrawal *Fiber-Optic Comminication Systems*, Willey Interscience 2010.
[28] D. Bimberg, M. Grundmann and N. N. Ledentsov, *Quantum Dot Heterostructures*, Wiley, New York, 1999.
[29] F. Capasso, C. Gmachl, D. L. Sivco, and A. Y. Cho, *Physics Today* **55**, 34 (2002).
[30] M.B. Spencer and W.E. Jr. Lamb, *Phys. Rev. A*, **5**, 884-892 (1972)
[31] A.A. Bakasov and N.B. Abraham, *Phys. Rev. A*, **4**8, 1633-1660 (1993).
[32] A. Gavrielides, V. Kovanis, and T. Erneux, *Opt. Comm.*, **1**36, 253-256 (1997).
[33] E. Ott, *Chaos in Dynamical Systems*, Cambridge University Press, 2002.
[34] Y. A. Kuznetsov, *Elements of Applied Bifurcation Theory*, Springer-Verlag New York, 1995.
[35] E. Doedel, A. Champneys, T. Fairgrieve, Yu.A. Kuznetsov, B. Sandstede, and X. Wang, AUTO 200: Continuation and bifurcation software for ordinary differential equations. Available via http://indy.cs.concordia.ca/auto/main.html.
[36] R. Lang and K. Kobayashi, *IEEE Journal of Quantum Electronics*, **Q**E-16(3), 347-355 (1980).
[37] K. Engelborghs, T.Luzyanina, G. Samaey, DDE-BIFTOOL v. 2.00: a Matlab package for bifurcation analysis of delay differential equations. Available from http://twr.cs.kuleuven.be/research/software/delay/ddebiftool.shtml.